Cellular Signalling 27 (2015) 245–256

Contents lists available at ScienceDirect

Cellular Signalling

journal homepage: www.elsevier.com/locate/cellsig

NKD1 marks intestinal and liver tumors linked to aberrant Wnt signaling

Jitka Stancikova [a,d,1,2], Michaela Krausova [a,2], Michal Kolar [a], Bohumil Fafilek [a], Jiri Svec [a,b], Radislav Sedlacek [a], Magdalena Neroldova [c], Jan Dobes [a], Monika Horazna [a], Lucie Janeckova [a], Martina Vojtechova [a], Martin Oliverius [c], Milan Jirsa [c], Vladimir Korinek [a,*]

[a] Institute of Molecular Genetics, Academy of Sciences of the Czech Republic, Videnska 1083142 20 Prague 4, Czech Republic
[b] Second Department of Internal Medicine, Third Faculty of Medicine, Charles University, Prague, Srobarova 50, 100 34 Prague 10, Czech Republic
[c] Institute for Clinical and Experimental Medicine, Videnska 1958/9, 140 21 Prague 4, Czech Republic
[d] Faculty of Science, Charles University in Prague, Albertov 6, 128 43 Praha 2, Czech Republic

ARTICLE INFO

Article history:
Received 17 August 2014
Received in revised form 24 October 2014
Accepted 8 November 2014
Available online 14 November 2014

Keywords:
Wnt signaling
NKD1
Intestine
Liver
Colorectal cancer
Hepatocellular carcinoma

ABSTRACT

The activity of the Wnt pathway undergoes complex regulation to ensure proper functioning of this principal signaling mechanism during development of adult tissues. The regulation may occur at several levels and includes both positive and negative feedback loops. In the present study we employed one of such negative feedback regulators, naked cuticle homolog 1 (Nkd1), to follow the Wnt pathway activity in the intestine and liver and in neoplasia originated in these organs. Using lineage tracing in transgenic mice we localized *Nkd1* mRNA to the bottom parts of the small intestinal crypts and hepatocytes surrounding the central vein of the hepatic lobule. Furthermore, in two mouse models of intestinal tumorigenesis, *Nkd1* expression levels were elevated in tumors when compared to healthy tissue. We utilized a collection of human intestinal polyps and carcinomas to confirm that *NKD1* represents a robust marker of neoplastic growth. In addition, expression analysis of *NKD1* in liver cancer showed that high expression levels of the gene distinguish a subclass of hepatocellular carcinomas related to aberrant Wnt signaling. Finally, our results were confirmed by bioinformatic analysis of large publicly available datasets that included gene expression profiling and high-throughput sequencing data of human colon and liver cancer specimens.

1. Introduction

The Wnt pathway represents one of the principal signaling mechanisms regulating development and tissue homeostasis in metazoan species. In the adult organism, aberrant Wnt signaling is involved in various diseases including cancer (reviewed in [1]). The central mediator of the best studied so-called canonical Wnt pathway is β-catenin, a protein playing a dual role in cell adhesion and signaling (reviewed in [2]). In the absence of an extracellular Wnt stimulus the β-catenin destruction complex, which is composed of casein kinase 1 alpha (CK1α) and glycogen synthase kinase 3 (GSK3), and scaffolding proteins adenomatous polyposis coli (Apc) and axin/conductin, phosphorylates β-catenin on the N-terminal serine/threonine residues. The phosphorylated protein is ubiquitinylated and subsequently degraded by the proteasome. Consequently, in unstimulated cell, the cytoplasmic levels of β-catenin remain low. Interaction of Wnt ligand with the receptor complex comprised of the Frizzled receptor and low-density lipoprotein receptor-related protein 5/6 (LRP5/6) co-receptor disrupts the function of the destruction complex. Subsequently, β-catenin accumulates in the cytoplasm and in the nucleus, where it associates with transcription factors of the lymphoid enhancer-binding factor/T-cell factor (LEF/TCF) family (further referred to as TCFs). Since β-catenin contains a transactivation domain, the TCF-β-catenin complexes act as bipartite transcriptional activators of the Wnt-responsive genes, such as *Axin2*, *c-Myc*, *CD44* or *cyclin D1* (for more comprehensive survey about the Wnt signaling target genes refer to the Wnt signaling home page: http://web.stanford.edu/group/nusselab/cgi-bin/wnt/target_genes).

Abbreviations: APC, adenomatous polyposis coli; BAC, bacterial artificial chromosome; CBC, crypt base columnar; Cp, crossing point; CRC, colorectal carcinoma; CTNNB1, the *β-CATENIN* gene; Dvl, dishevelled; EGFP, enhanced green fluorescent protein; EphB2, ephrin type-B receptor 2; GI, gastrointestinal; GS, glutamine synthetase; HBV, hepatitis B virus; HCC, hepatocellular carcinoma; HCV, hepatitis C virus; ISC, intestinal stem cell; ISH, *in situ* hybridization; LacZ, β-galactosidase; Lgr5, leucine-rich repeat containing G protein-coupled receptor 5; Min, multiple intestinal neoplasia; Nkd, naked cuticle homolog; Olfm4, olfactomedin 4; PCA, principal component analysis; qRT-PCR, reverse-transcription quantitative polymerase chain reaction; SD, standard deviation; TA, transit amplifying; TCF, T-cell factor; TCGA, The Cancer Genome Atlas.

* Corresponding author at: Institute of Molecular Genetics AS CR, Videnska 1083, 142 20 Prague 4, Czech Republic. Tel.: +420 241063146; fax: +420 244472282.
E-mail address: korinek@img.cas.cz (V. Korinek).

[1] Affiliation to the Faculty of Science is related to the support of the first author from the Grant Agency of Charles University in Prague; none of the results presented in this article were generated, obtained, or analyzed in relation to this affiliation.

[2] These authors contributed equally to this work.

http://dx.doi.org/10.1016/j.cellsig.2014.11.008

The intestinal epithelium represents one of the most dynamic tissue in mammalian body (reviewed in [3]). The single-layer epithelium of the small intestine is formed by microscopic projections into the intestinal lumen called villi, and invaginations into underlying mesenchyme, so-called crypts of Lieberkühn. Tissue homeostasis is maintained by intestinal stem cells (ISCs) residing in the bottom part of the crypts. ISCs divide asymmetrically, giving rise to fast-cycling transit amplifying (TA) cells located above the stem cell zone. Descendants of TA cells move up along the crypt/villus axis. At the crypt orifice these cells differentiate to generate specialized cell lineages of the gut that mainly include absorptive enterocytes, mucus-secreting goblet cells, and enteroendocrine cells producing hormones. Differentiated cells continue their movement up to the top of the villus, where they are extruded to the intestinal lumen. The process of epithelial self-renewal is completed in 3–5 days. One exception from this scheme are Paneth cells. The life span of these cells is 6–8 weeks. Furthermore, mature Paneth cells do not migrate from the crypt but stay at the crypt bottom, where they produce antibacterial cryptidins, defensins, and lysozyme (reviewed in [4]). The tissue architecture of the colon reminds the small intestine; however, it does not contain Paneth cells and its surface is flat without the extruding villi. ISCs, alternatively named according to their slender appearance and localization in the lower portion of the crypt as crypt base columnar (CBC) cells, can be recognized by expression of leucine-rich repeat containing G protein-coupled receptor 5 (Lgr5) [5]. Recently, several other markers of ISCs were discovered. These include the tumor necrosis factor receptor family member Troy [6], transcription regulator achaete-scute complex homolog 2 (Ascl2), and an extracellular matrix glycoprotein, olfactomedin 4 (Olfm4) [7]. In addition, CBCs produce high levels of transmembrane ephrin type-B receptor 2 (EphB2), whose expression declines in TA cells, and Paneth cells are EphB2 negative [8].

A number of studies established the Wnt pathway as the main constituent of the signaling network regulating ISCs pluripotency and proliferation (reviewed in [9]). For example, the expression of stem cell markers *Ascl2*, *Lgr5* and *Troy* is governed by the canonical Wnt pathway. Moreover, genetic disruption of genes encoding the Wnt pathway effectors *Tcf4* [10,11] or *β-catenin* [12,13] is associated with demise of intestinal crypts. Interestingly, Wnt/β-catenin signaling plays a key role in the metabolic zonation of the liver (reviewed in [14]). To fulfill its metabolic function, the liver tissue is organized into hepatic lobules, hexagonal-shaped functional units of hepatic parenchyma composed of 15–25 cells. The hepatocytes in the center of the lobule are called perivenous, since they surround a hepatic centrilobular vein. The outer row of lobular hepatocytes line the portal space. These periportal cells are in close contact with the so-called portal triad consisting of the hepatic artery, portal vein and bile duct. Consequently, the periportal hepatocytes receive a mixture of blood originating from both vessels. The portocentrovenular axis of the lobule is the basis for the zonation of the metabolic functions in the adult organ. Cells in different areas of the hepatic lobule are not equal, but they express different genes involved in the metabolism of carbohydrates, xenobiotics, bile production, and detoxification of ammonia. The perivenous hepatocytes contain nuclear β-catenin and they display active Wnt signaling. The Wnt pathway regulates genes encoding enzymes of ammonia detoxication and transport. The genes include *glutamine synthetase* (*GS/Glul*), *ornithine aminotransferase* (*Oat*), and *leukocyte cell-derived chemotaxin-2* (*Lect2*). In contrast, high Apc protein levels in the periportal hepatocytes suppress the Wnt pathway activity. This leads to production of a different set of enzymes mainly participating in ammonia, urea, and carbohydrate metabolism such as *glutaminase 2* (*Gls2*), *arginase 1*, and *phosphoenolpyruvate carboxykinase 1* (*Pck1*) [15].

Aberrant Wnt signaling is found in a multitude of solid tumors, particularly in carcinoma of the colon and rectum [colorectal carcinoma (CRC) [reviewed in [16]]. It is assumed that in the majority of sporadic CRCs the "driver" mutation providing selective advantage to the prospective cancer cell occurs in the *APC* tumor supressor [17,18]. The mutational changes in *APC* lead to production of truncated APC polypeptide that compromises proper functioning of the β-catenin destruction complex (reviewed in [19]). The Wnt pathway might also be activated by inactivating mutations in *AXIN1* [20] or *AXIN2* [21]. In addition, approximately 5% of CRCs contain oncogenic mutations in the *CTNNB1* gene (this gene encodes β-catenin) that alter regulatory amino acid residues at the β-catenin N-terminus and stabilize the protein [22]. The most common type of liver cancer is hepatocellular carcinoma (HCC). The etiology of the disease is heterogeneous and is frequently linked to hepatitis B virus (HBV) or hepatitis C virus (HCV) chronic infection or to alcoholism-related cirrhosis (reviewed in [23]). Recently, several studies performed gene expression profiling and/or high-throughput DNA sequencing to identify the molecular subclasses of HCC or to detect the driver mutations related to liver carcinogenesis [24,25]. Importantly, approximately one-half of HCCs display elevated expression levels of genes activated by Wnt signaling, and oncogenic mutations in the *CTNNB1* gene are found in 20-30% of all HCCs. Analogically to CRC, high levels of stabilized β-catenin and inappropriate transcriptional activation of the TCF-β-catenin target genes is a hallmark of a significant portion of HCCs (reviewed in [26]).

In our previous study we employed chromatin immunoprecipitation in combination with DNA microarray analysis (so-called ChIP-on-chip) to identify genes activated by aberrant Wnt/β-catenin signaling in human CRC cells. One of the genes bound by the TCF4-β-catenin complexes was *naked cuticle homolog 1* (*NKD1*) [6]. Nkd1 is an evolutionarily conserved feedback inhibitor of the Wnt pathway [27]. It interacts with dishevelled (Dvl1) and mediates degradation of this cytoplasmic Wnt signal transducer [28]. Nkd1 reduces aberrant Wnt signaling; nevertheless, in the absence the excessive Wnt signal, its function is less apparent [29,30]. Simultaneous inactivation of both vertebrate paralogs *Nkd1* and *Nkd2* in the mouse leads to only subtle alterations in the morphology of cranial bones and slightly reduced litter size, but the mice are otherwise normal [31]. Based on these and other results mainly obtained in zebrafish [30], Angonin and Van Raay proposed that Nkd1 functions as a "passive antagonist" that acts only when the Wnt signaling levels exceed some threshold [32].

In the present study, we analyzed the *Nkd1* expression pattern in adult mouse gut and liver tissue. Using lineage tracing approaches in transgenic animals we show that *Nkd1* expression is confined to the areas with active Wnt signaling. Furthermore, *Nkd1* transcription was robustly increased in tumors developed in multiple intestinal neoplasia (Min) of mice or in hyperplastic crypts generated by conditional deletion of the *Apc* gene. Using a panel of sporadic tumors of the colon we confirmed that elevated expression of *NKD1* marks neoplastic tissue. In hepatic neoplasia, high *NKD1* mRNA levels, together with upregulation of *AXIN2*, *EPHB2*, and *GS*, distinguish a class of HCCs with deregulated Wnt signaling.

2. Materials and methods

2.1. Experimental animals

$Apc^{+/Min}$ [33,34], Lgr5-EGFP- IRES-CreERT2 [5], Rosa26R [35], and Rosa26R-EYFP [36] mice were purchased from the Jackson Laboratory (Bar Harbor, ME). $Apc^{cKO/cKO}$ [37] mice were obtained from the Mouse Repository (National Cancer Institute, Frederick, MD). Villin-CreERT2 mice [38] were kindly provided by Sylvia Robine (Institut Curie, Paris, France). Animals were housed and handled according to the guidelines approved by the institutional committee. Tamoxifen (Sigma-Aldrich, St. Louis, MO) administration was done by intraperitoneal injection of 1 mg of the compound dissolved in 0.1 ml of corn oil. DNA from tail clippings was used for genotyping. Tissue samples were digested in Proteinase K solution (Thermo Fisher Scientific, Waltham, MA) and precipitated using ethanol; pellets were dissolved in 20 μl of TE buffer (10 mM Tris-HCl, 1 EDTA, pH 8) and 1 μl was used for PCR performed with DreamTaq PCR Master Mix (Thermo Fisher Scientific, Waltham, MA).

2.2. Generation of Nkd1-CreERT2 transgenic mice

The Nkd1-CreERT2 bacterial artificial chromosome (BAC) transgenic construct was generated using homologous recombination in bacteria according to the previously published protocol [39]. The BAC clone RP23-301 N2 was purchased from imaGenes (Berlin, Germany); a construct containing CreERT2 cDNA was kindly provided by M. Cepko via Addgene. The adapters "a" (5′-TCCTTTCTTTCCGGCTCCCGCCGCCGCCGC CGCGCGCGATGTGCCCGCAGCCatgtccaatttactgaccgtac- 3′; the *Nkd1*-specific sequence is capitalized, the part complementary to the CreERT2 expression cassette is given in lowercase) and "b" (5′-AGAGACCAAGTT CTCCGGAGTAGGGGCTGGCGACTAGAGGAAGGCGCAAGTGGCGGCCGC TCTAGAACTAGTG- 3′) were derived from the sequence of the *Nkd1* second exon. The adapters were employed for PCR amplification, the product was purified from agarose gel and electroporated into the *E. coli* strain EL250 harboring the BAC clone. Bacterial clones containing correctly recombined BACs were verified by PCR. Isolated recombinant BAC DNA was linearized and used for pronuclear injection of fertilized eggs (C57Bl/6 J background). Two Nkd1-CreERT2 transgenic founder lines were produced using the service of the Transgenic Unit of the Institute of Molecular Genetics (IMG). Two lines exhibited a virtually identical pattern of the Cre recombinase activity.

2.3. X-gal staining, immunohistochemistry, antibodies, and periodic acid-Schiff (PAS) staining

Mouse tissues were stained with X-gal (Amresco, Solon, OH) prior to paraffin embedding. Tissue processing and staining was performed as described previously [5]. Slides were immersed in a steam bath (20 min, 10 mM citrate buffer, pH 6) for antigen retrieval. The following rabbit polyclonal antibodies were used for immunohistochemistry: anti-chromogranin A (cat. No. ab15160, Abcam, Cambridge, UK), anti-lysozyme (cat. No. A0099, Dako, Glostrup, DK), anti-glutamine synthetase (cat. No. ab73593, Abcam). PAS (Diapath, Martinengo, IT) staining was performed according to the standard protocol provided by the supplier. Slides were counterstained using either hematoxylin (Penta, Prague, CZ) or nuclear fast red (Diapath, Martinengo, IT).

2.4. RNA probes and in situ hybridization (ISH)

Both sense and antisense RNA probes were derived from the following regions of the analyzed genes: *Axin2* (accession: NM_015732.4), nucleotides (nt) 2069-2938; *Nkd1* (NM_001163660.1), nt 509-944. DNA fragments encompassing the indicated regions were subcloned into pBluescript SK II (Stratagene, La Jolla, CA). The constructs were linearized, and digoxigenin-labeled antisense RNA and control sense probes were generated from the template using the DIG RNA Labeling Kit (Roche Applied Science, Basel, Switzerland). Dissected small intestinal and liver tissue was embedded in O.C.T. medium (Tissue-Tek, Sakura Finetek Europe B.V., The Netherlands). Ten μm sections were cut and mounted on Super Frost Plus slides (Electron Microscopy Sciences, Hatfield, PA). Sections were post-fixed in 4% (w/v) paraformaldehyde in phosphate-buffered saline (PBS; 4 °C, 10 min), acetylated for 10 min (acetic anhydride, 0.25%; Sigma-Aldrich) and hybridized with digoxigenin-labeled probes overnight at 62 °C. ISH was carried out as described previously [40]. Whole-mount ISH was performed according to the protocol of Cepko and Tabin (http://genepath.med.harvard.edu/~cepko/protocol/ctlab/ish.ct.htm).

2.5. Isolation of intestinal crypt cells and hepatocytes, fluorescence-activated cell sorting (FACS)

Crypts from the proximal part of the small intestine of Lgr5-EGFP-IRES-CreERT2 mice were isolated according to the protocol published previously [41]. Single-cell suspension was obtained upon incubation of fresh crypts with dispase I (0.8 mg/ml, 10 min at 37 °C; Sigma-Aldrich) and passing the resulting suspension through 70-μm strainer (Fisher Scientific, Waltham, MA). Cell suspension was stained by biotinylated *Ulex europaeus* agglutinin I (UEA I) (Vector Laboratories, Burlingame, CA) and streptavidin-PE-Cy7 (BD Biosciences, Mississauga, ON). Hepatocytes were isolated from perfused liver of Nkd1-CreERT2^{+}/Rosa26R-EYFP mice as described previously [42]. The animals were injected twice (with 24-hour interval between injections) with tamoxifen (1 mg in 100 μl of corn oil per dose) and utilized the next day upon the second injection.

2.6. RNA isolation and reverse-transcription quantitative polymerase chain reaction (qRT-PCR)

Total RNA was extracted from tissues or sorted cells using RNAeasy MiniKit with DNase treatment (Qiagen, Hilden, Germany) following the manufacturer's instructions and reverse transcribed using MAXIMA reverse transcriptase (Thermo Fisher Scientific, Waltham, MA). The LightCycler 480 apparatus and SYBR Green I Master Mix (Roche Applied Science) were employed for qRT-PCR. Primers are listed in Supplementary Table S1.

2.7. Collection and analysis of human colorectal lesions

The study was approved by the Clinical and Experimental Medicine and the Thomayer University Hospital Research Ethics Committee and the Ethics Committee of the Third Faculty of Medicine, Charles University in Prague. Processing and histopathological evaluation of samples of 35 precancerous and 20 malignant lesions of colorectal tissue were described in full detail previously [6]. Briefly, genomic DNA and total RNA was isolated from tumor segments and matched healthy mucosa. RNA was reverse transcribed and used for qRT-PCR analysis; PCR reactions were run in triplicates with two negative controls (RT reactions in which reverse transcriptase was omitted). Mutational analysis of the *APC* gene was performed with genomic DNA extracted from CRC specimens only. To obtain relative expression levels (-ΔCp) (Cp indicates the crossing point value), individual Cp values were normalized by geometric average of internal housekeeping genes *β-ACTIN* (*ACTB*), *UBIQUITIN B* (*UBB*) and *AXIN1* (premalignant lesions of the colon), or using *ACTB* as a sole reference gene (CRC-derived samples). Differential expression was examined by non-parametric Wilcoxon's rank-sum test. In addition, the individual background of the patients was encompassed in a REML-fitted linear model, described by the formula ΔCp ~ patient + tissue/(stage * *APC* mutation) for CRC specimen and ΔCp ~ patient + tissue_stage in cases of precancerous lesions, respectively. Biopsies of surrounding non-tumor tissue constitute a single group (ΔΔCp) in both collections. In corresponding figures and tables, the number of asterisks represents statistically significant changes with the following P values: *$P < 0.05$, **$P < 0.01$, and ***$P < 0.001$. All analyses were performed in R language. Primer sequences are listed in Supplementary Table S1.

2.8. Collection and analysis of human hepatic lesions

Neoplastic liver tissues were obtained from 28 consecutive patients at the time of surgical resection performed at the Transplant Surgery Department of the Institute for Clinical and Experimental Medicine. Collection of clinical samples was accomplished in concordance with the standards and approved by the Institute for Clinical and Experimental Medicine and Thomayer University Hospital Research Ethics Committee; all study subjects signed the informed consent. The paired, non-tumor tissue specimens were used as controls. Histopathology was scored in hematoxylin and eosin stained sections by two independent pathologists; clinical characteristics are given in Supplementary Table S2. Diagnoses of HCC were predominant within the cohort. Total RNA was purified using the RNeasy Mini kit in automated QIAcube extractor (Qiagen). Reverse transcription was performed with 250 ng of

input RNA using RevertAid H Minus First Strand cDNA Synthesis kit supplied with 25 ng/μl oligo(dT)$_{18}$ primers (Thermo Scientific). PCR reactions were run in triplicates using Light Cycler 480. Relative expression levels (-ΔCp) were obtained upon normalization by geometric average of internal housekeeping genes *ACTB* and *UBB*. To detect differences in expression, we employed Wilcoxon's rank-sum test and, in addition, the linear model (REML) described by the formula ΔCp ~ patient + tissue_fibrosis score. Statistical significance levels were set identically to CRC samples.

2.9. CTNNB1 mutation analysis in HCC

Genomic DNA was purified from snap-frozen samples of tumor and matched surrounding tissue using DNeasy Blood & Tissue Kit (Qiagen). Exon 3 of *CTNNB1*, including intron-exon boundaries, was amplified using gene-specific primers: forward: 5′taatac gactcactatag TGCTTTTCTTGGCT GTCTTTCAG 3′; reverse: 5′tgaaa cagctatgaccatgTCCACAGTTCAGCATTTACCTAAG 3′; overhang sequences corresponding to universal sequencing primers T7 and RP, respectively, are given in lowercase letters. Each fragment was directly sequenced from both sides using the BigDye® Terminator v3.1 cycle sequencing kit and ABI 3130 Genetic Analyzer (Applied Biosystems, Life Technologies, Prague, Czech Republic).

2.10. CRC and HCC datasets obtained from The Cancer Genome Atlas (TCGA)

CRC [TCGA_COADREAD; 154 cases of colon cancer (dataset COAD-TP); 73 cases of rectal cancers, (dataset READ-TP)] [18] and HCC (TCGA_LIHC; 197 cases) datasets were downloaded from the Broad Institute using the utility firehose_get (http://gdac.broadinstitute.org, Broad Institute/Massachusetts Institute of Technology, USA) on July 18, 2014. RNA-seq data were extracted from the archive "gdac.broadinstitute.org_COADREAD.Merge_rnaseqv2__illuminaga_rnaseqv2__unc_edu__Level_3__RSEM_genes_normalized__data.Level_3.2014061400.0.0" (CRC) and "gdac.broadinstitute.org_LIHC.Merge_rnaseqv2__illuminahiseq_rnaseqv2__unc_edu__Level_3__RSEM_genes_normalized__data.Level_3.2014061400.0.0" (HCC). Mutation data were obtained from the archive: "gdac.broadinstitute.org_COADREAD.Mutation_Packager_Calls.Level_3.2014061400.0.0" (CRC) and "gdac.broadinstitute.org_LIHC.Mutation_Packager_Calls.Level_3.2014061400.0.0" (HCC). Clinical data were retrieved from the files: "gdac.broadinstitute.org_COADREAD.Merge_Clinical.Level_1.2014061400.0.0/COADREAD.clin.merged.txt" (CRC) and "gdac.broadinstitute.org_LIHC.Merge_Clinical.Level_1.2014061400.0.0/LIHC.clin.merged.txt" (HCC). No further processing was applied to the data. In CRC datasets only samples classified as colon cancer (COAD) and with a determined mutation status of the *APC* gene (104 cases) are presented. DNA methylation data were retrieved from the file: "gdac.broadinstitute.org_COADREAD.Merge_methylation__humanmethylation450__jhu_usc_edu__Level_3__within_bioassay_data_set_function__data.Level_3.2014061400.0.0". Only those data subsets were analyzed that had both expression and methylation data available (366 cases). Positions of the CpG-islands predicted by the algorithm of Wu and colleagues [43] were obtained from the file: "http://rafalab.jhsph.edu/CGI/model-based-cpg-islands-hg19.txt" (accessed on September 8, 2014). North and south shores (N/S-shores) were defined as chromosomal regions flanking the corresponding CpG island 2 kb upstream or downstream, respectively. North/south shelves (N/S-shelves) were defined as chromosomal regions flanking the shores further 2 kb upstream/downstream [44]. Base 2 logarithm of fold change (logFC) of *NKD1* expression intensity between tumor samples and the median of available normal tissue samples was determined. The CRC samples were clustered according to methylation β-values (methylated/overall intensity) for the probes assigned to the *NKD1* gene (**Infinium Human Methylation** 450 array, Illumina). All analyses were performed in the R environment.

3. Results

3.1. Nkd1 expression marks Apc-deficient intestinal tumors in the mouse

To analyze *Nkd1* expression in mouse tumors we performed ISH using specimens obtained from Min mice. These mice (designated Apc$^{+/Min}$) harbor a nonsense mutation in the coding region of the *Apc* gene and all adult animals develop numerous Apc-deficient polyps that progress to malignancy [34]. *Nkd1* mRNA was clearly detected in the small intestinal tumors; nevertheless, we did not observe any

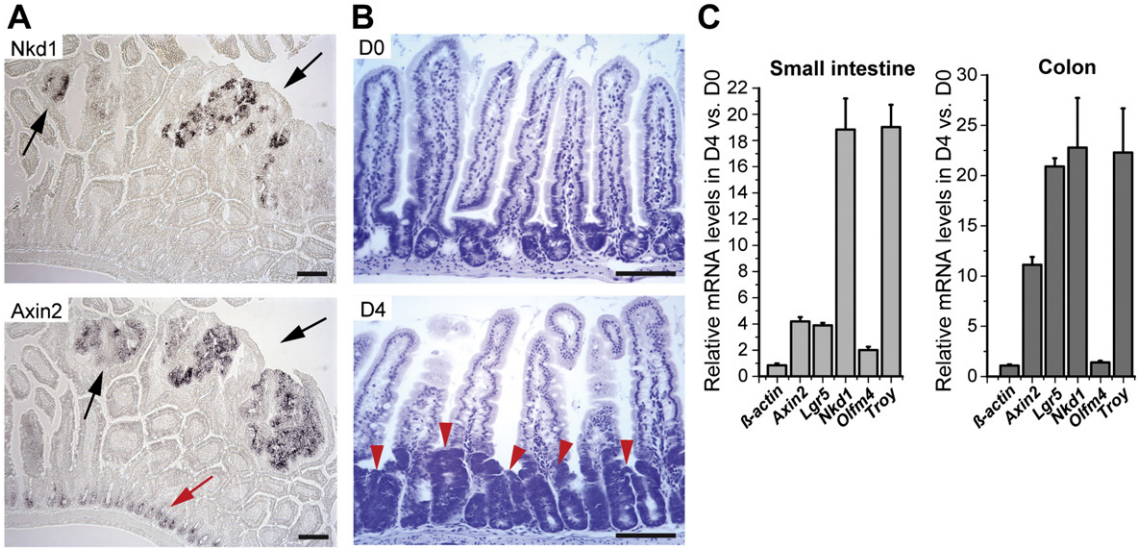

Fig. 1. *Nkd1* mRNA is enriched in mouse intestinal tumors. (A) ISH of *Axin2* and *Nkd1* mRNAs in small intestinal tumors (black arrows) of Apc$^{+/Min}$ mice. In the healthy part of the tissue *Axin2* was also detected in lower parts of the crypts (red arrow). (B) Conditional deletion of the *Apc* allele results in crypt hyperplasia. Hematoxylin-stained sections of the jejunum of Villin-CreERT2^{+}/Apc$^{cKO/cKO}$ mice obtained at day 0 (D0) and day 4 (D4) after tamoxifen administration. Hyperproliferative crypts are indicated by red arrowheads. Scale bar: 0.1 mm. (C) Quantitative RT-PCR analysis of total RNA isolated from crypts at D0 and D4. The results were normalized to *Ubiquitin B* (*Ubb*) mRNA levels; another housekeeping gene, *β-actin*, was also included in the test. The expression level of a given gene in the crypt cells at D0 was arbitrarily set to 1. Error bar: standard deviation (SD).

(specific) *Nkd1* signal in non-neoplastic tissue. This was in contrast to *Axin2*, which was clearly enriched not only in tumors, but also at the bottom of the intestinal crypts (Fig. 1A). To confirm that *Nkd1* expression is directly connected to the loss of *Apc* we employed animals harboring conditional alleles (cKO) of this tumor suppressor. Cre-mediated excision of the floxed exon 14 in $Apc^{cKO/cKO}$ mice results in production of a truncated polypeptide related to nonfunctional Apc protein produced in $Apc^{+/Min}$ mice [37]. The *Apc* gene inactivation was performed in Villin-CreERT2^{+}/$Apc^{cKO/cKO}$ mice expressing tamoxifen-regulated Cre enzyme throughout the epithelia of the gastrointestinal tract [38]. As expected, robust hyperplasia of the small intestinal and colonic crypts was observed several days upon tamoxifen administration (Fig. 1B and data not shown). Quantitative RT-PCR analysis of crypt cells isolated from animals prior and four days after tamoxifen treatment showed more than 18- and 20-fold increase in the *Nkd1* mRNA levels in the Apc-deficient small intestine and colon, respectively. Wnt signaling target genes *Axin2*, *Lgr5*, and *Troy* were also upregulated. In contrast, transcription of *Olfm4*, a marker of small intestinal stem cells which is not driven by active Wnt signaling [7], was slightly elevated in the hyperproliferative crypts isolated from the small intestine and not from the colon (Fig. 1C).

3.2. Nkd1 is produced in the Wnt-responsive areas of the small intestine and liver

Next we analyzed the distribution of Nkd1 in the healthy gut tissue. Since the localization of *Nkd1* mRNA and protein using ISH or immunohistochemical staining was inconclusive, we used transgenesis to follow the expression pattern of the gene. BAC carrying the mouse *Nkd1* locus was employed to generate Nkd1-CreERT2 transgenic mice. In the BAC-based construct, cDNA encoding tamoxifen-inducible Cre enzyme was inserted into the second exon of the *Nkd1* gene. The insertion is in frame with the translation start codon located in the preceding exon (Fig. 2A). The activity of CreERT2 recombinase produced from the Nkd1-CreERT2 BAC transgene was visualized in embryos derived from crossing Nkd1-CreERT2 and Rosa26R mice. Rosa26R animals express bacterial *β-galactosidase* (*LacZ*) mRNA from the ubiquitously active *Rosa26* allele. The mRNA is not translated unless a transcriptional blocker flanked by two loxP sites is excised by Cre [35]. Developing embryos removed from pregnant females one day after tamoxifen injection were used to stain the LacZ-expressing tissue. Importantly, the expression pattern of Nkd1-CreERT2 visualized by the chromogenic X-gal substrate phenocopied the sites of expression of endogenous *Nkd1* mRNA obtained by whole-mount ISH (Fig. 2B). Furthermore, the sites of the CreERT2 activity were in agreement with the previously described *Nkd1* expression pattern [31].

Subsequently, adult Nkd1-CreERT2^{+}/Rosa26R mice were injected with a single dose of tamoxifen and sacrificed at several time points later. In the gastrointestinal (GI) tract, Cre-mediated recombination was the most efficient in the duodenum and jejunum, much less effective in the ileum, and virtually no staining was observed in the colon (Fig. 2C). Since we [6] and others [45] observed that Cre-mediated recombination is less efficient in the distal parts of the GI tract, we supposed that the observed variability in LacZ staining was caused by the inefficient recombination of the floxed blocker rather than heterogeneous expression of *Nkd1*. Therefore, the histological analysis was performed using specimens obtained from the proximal part of the small intestine. One day after the Cre induction, cells producing LacZ were located in the lower parts of the crypts (Fig. 2D). Two distinct staining patterns were observed seven days after the recombination. Some of "blue" cell clones started to extend along the whole crypt axis. However, other clones separated from the crypts and moved as a stripe of cells on the villus, indicating that the recombined cell was possibly a TA cell. Finally, three weeks after recombination, continuous "ribbons" of labelled cells emanating from the crypts and reaching the top of the villi were observed. In addition, blue cells were also found at the bottom of the crypts, i.e. in the positions where mature Paneth cells are localized (green arrow in Fig. 2D). Importantly, Nkd1-CreERT2-expressing cells differentiated into all major cell lineages present in the small intestine (Fig. 2E). The recombined clones persisted in the small intestine for more than two months, confirming that besides Paneth and TA cells some CreERT2-positive cells are indeed ISCs (not shown). To verify that the Nkd1-CreERT2 activity mimics expression of endogenous *Nkd1*, crypt cells obtained from Lgr5-EGFP-IRES-CreERT2 mice were sorted and analyzed using qRT-PCR. Lgr5-IRES-EGFP-CreERT2 animals express enhanced green fluorescent protein (EGFP) from the *Lgr5* locus, and therefore the EGFP protein can be used as a surrogate marker of ISCs [5]. Besides EGFP florescence, cell labeling with UEA I lectin was applied. The lectin binds proteoglycan residues on the surface of secretory cell lineages including Paneth cells and their precursors. Crypts isolated from the jejunum were used for the sorting procedure since this part of the small intestine contains only a minimal count of UEA I-positive goblet cells [46]. The highest *Nkd1* expression (when compared to TA cells negative for UEA and GFP) was detected in mature Paneth cells (phenotype: UEA^{+}GFP^{-}cryptidines^{+}) and Lgr5^{+} ISCs (UEA^{-}GFP^{+}EphB2^{+}), although expression of cryptidines in the latter population indicated that we did not obtain a homogenous cell population. Interestingly, high levels of *Nkd1* mRNA were also detected in putative progenitors of the Paneth cell lineage that are positive for UEA and GFP, and produce Lgr5 and cryptidins as well [46]. The result was consistent with the frequency of blue cells detected by immunohistochemical staining of crypts in Nkd1-CreERT2^{+}/Rosa26R mice one day after tamoxifen administration (Fig. 2G).

Since previous reports indicated *Nkd1* expression in pericentral hepatocytes [31], we followed the Nkd1-CreERT2 activity in adult liver tissue. One day after tamoxifen administration, X-gal staining was detected in hepatocytes surrounding the putative central vein (Fig. 3A). The identity of LacZ-positive cells was subsequently confirmed by co-staining with an antibody recognizing GS, a robust marker of pericentral hepatocytes (Fig. 3B). Additionally, we intercrossed Nkd1-CreERT2 animals with Rosa26R-EYFP reporter mice that express enhanced yellow fluorescent protein (EYFP) instead of LacZ from the *Rosa26* locus [36]. We performed gene expression profiling of total RNA isolated from EYFP-positive and EYFP-negative hepatocytes sorted from these mice. The analysis confirmed that endogenous *Nkd1* mRNA is robustly enriched in EYFP^{+} cells along with the perivenous hepatocyte-specific genes *GS*, *Lect2*, and *Oat*. In accordance with the literature, these cells also produce increased levels of *Axin2* mRNA [15]. *Apc* and the "housekeeping" gene *glyceraldehyde-3-phosphate dehydrogenase* (*GAPHD*) did not show any differential distribution among the sorted cell populations; however, the periportal *Pck1* gene displayed an inverse expression pattern to the perivenous genes, confirming the quality of the sorting procedure (Fig. 3C).

3.3. Elevated levels of NKD1 mRNA in sporadic premalignant lesions of the colon and in CRC

As a next step, we examined the expression pattern of human *NKD1* in tumors arising in the gut. In dysplastic premalignant stages of CRC, we observed robust upregulation of *NKD1* expression. The increase in *NKD1* mRNA abundance showed an ascending tendency as the lesions progressed towards more advanced phenotypes. In contrast, in hyperplastic polyps *NKD1* transcription was significantly decreased when compared to the matched healthy mucosa (Fig. 4A). In CRC the elevated *NKD1* expression occurred irrespective of the *APC* mutational status and hence resembled deregulation of *LGR5* (Fig. 4B) [6].

To explore the alterations in *NKD1* transcription in a larger panel of CRCs, we interrogated relevant datasets from TCGA (227 specimens in total) [18]. The analysis was less straightforward, since the expression data obtained from healthy matched tissue were not accessible from these datasets. Intestinal cancers were stratified according to disease progression, and subsequently, the tumors were further subdivided using the classification system associated with the cellular phenotype

[47] or according to genetic stability [18]. In early-stage tumors *NKD1* mRNA was enriched (similarly to *AXIN2*) in microsatellite stable (MSS) lesions [when compared to lesions displaying low (MSI-L) or high (MSI-H) microsatellite instability (MSI)]. Moreover, in both early and advanced CRCs the *NKD1* transcript was abundant in the progenitor ("TA") type of tumors (Supplementary Fig. S1).

3.4. NKD1 transcription indicates HCC displaying aberrant Wnt signaling

The *NKD1* expression was analyzed in 28 neoplastic liver tissues obtained at the time of surgery. Paired, non-tumor tissue specimens were used as controls. Recently, Lachenmayer and colleagues employed expression data of 642 HCCs to define two classes of HCC displaying dysregulation of the Wnt pathway. The "Wnt class" is characterized by nuclear accumulation of β-catenin and upregulation of liver-specific Wnt signaling target genes. The "Wnt-TGFβ" class is defined by expression of a different set of genes (see further) regulated by Wnt signaling [25]. In the initial analysis we observed a clear separation of a fraction of the HCC samples into the Wnt class that was established by simultaneous upregulation of *AXIN2*, *EPHB2* and *GS*. However, we did not observe any clustering of HCCs to the Wnt-TGFβ class as examined by transcription levels of the *PLAU*, *MMP7*, *SALL1* and *RUNX2* genes (not shown). Thus, we stratified the HCC samples into subgroups defined by the Wnt-signature only. We employed the MCLUST algorithm [48] to group the samples according to their *AXIN2*, *EPBH2*, and *GS* Cp values. The algorithm identified four clusters, three of which showed low and

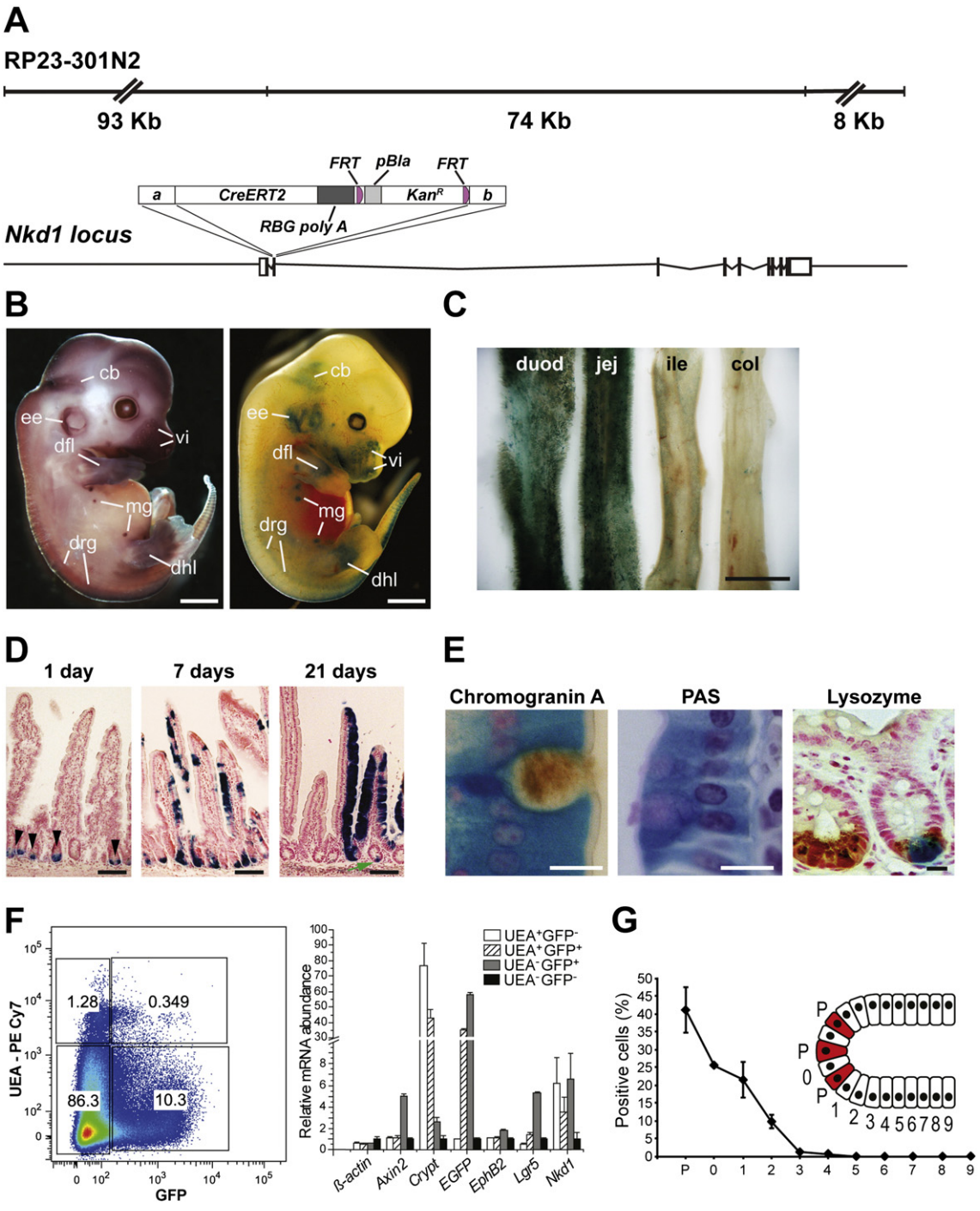

one (11 samples) exhibited high Wnt-signature "intensity". Due to small cluster sizes, we merged the Wnt signature-negative clusters into a single class and subsequently obtained two classes of HCC designated "HCC" and "HCC_Wnt" (Supplementary Fig. S2). An alternative clustering method, partitioning around medoids (with k = 2), resulted in virtually identical grouping (not shown). To further validate the result, we used the algorithm to predict the class of all other samples, i.e. healthy liver parenchyma, precancerous tissues, cholangiocellular carcinoma, and other than HCC liver neoplasia, which we expected to be negative for the Wnt-signature. Indeed, all these samples were correctly classified outside of the HCC_Wnt class (not shown). Finally, we analyzed the *CTNNB1* gene mutation status in genomic DNA obtained from all liver samples. The exon 3 sequence encoding amino acid residues regulating β-catenin protein stability was used for the analysis. Missense mutations in codons for regulatory serines/threonines (or in codons closely adjacent to these residues) were found in 11 HCCs; nine of these tumors were assigned to the HCC_Wnt class (Supplementary Table S3). Consistently, transcription levels of *NKD1* were positively correlated with expression of the genes defining the HCC_Wnt class (*AXIN2*, *EPHB2*, and *GS*), as well as with additional target genes of canonical Wnt/β-catenin signaling *LGR5* and *TROY*. In contrast, transcription of the paralogous *NKD2* gene, which is not regulated by the Wnt pathway, was not elevated in specimens assigned to the HCC_Wnt class (Fig. 5).

Next, we analyzed relevant HCC datasets from TCGA (197 specimens). The expression levels of the Wnt-signature genes *AXIN2*, *EPBH2*, and *GS* and the MCLUST algorithm were employed to group the HCC specimens. The algorithm identified three clusters of HCCs designated HCC_1 (12 samples), HCC_2 (148 samples), and HCC_Wnt (37 samples) (Supplementary Fig. S3). Additionally, we employed genomic DNA sequencing data to determine the *APC*, *AXIN1/2*, and *CTNNB1* mutational status (mutations were classified according to references [49, 50]). In the examined tumors *APC* was compromised in 3%, *AXIN1* in 5%, and *AXIN2* in 2% cases. In contrast, mutations activating *CTNNB1* occurred in 26% of specimens. Consistent with other studies [51], nonsynonymous gene alterations in either the *AXIN1* or *APC* tumor suppressors and *CTNNB1* were mutually exclusive, with only one specimen displaying concurrent oncogenic mutations in the *CTNNB1* exon 3 together with disruption of *AXIN2* (not shown). Since the HCC TCGA dataset contains exome sequencing data, we utilized the mutational status of the *APC*, *CTNNB1*, and *AXIN1/2* genes to divide all specimens to three mutation groups (designated "Wnt_WT", "Wnt_MUT", and "Other"). As expected, HCC_Wnt class-specific genes *AXIN2*, *EPHB2* and *GS* were robustly overexpressed in the Wnt_MUT group (sample count 38) defined by *CTNNB1* (activating) and *APC* (inactivating) mutations (Supplementary Fig. S4). Importantly, in the TCGA HCC1 samples *NKD1* transcription was also positively correlated with *AXIN2*, *EPBH2*, and *GS*, and, furthermore, *NKD1* mRNA was significantly enriched in the Wnt_MUT group (Fig. 6A). Interestingly, in five HCC specimens that were assigned to the HCC_Wnt expression class, no oncogenic mutations in *APC*, *CTNNB1*, and *AXIN1/2* were detected (one sample was assigned to the mutational subgroup "Other" and four other HCCs to the subgroup Wnt_WT) (Supplementary Table S4). Careful scrutiny of genomic DNA from the tumor in the "Other" group revealed that this lesion harbors a missense mutation (c.G417T/p.L139F) in exon 4 of the *CTNNB1* gene that possibly compromises the structural integrity of the first armadillo repeat of β-catenin. Consequently, the alteration might lead – by inhibiting phosphorylations by CK1 – to β-catenin stabilization and inappropriate signaling [52]. We investigated the molecular background of four other samples from the Wnt_WT mutation group. Interestingly, we detected increased levels of *LGR5* in these specimens. In addition, in two tumors, copy-number identified amplification of the *R-spondin 2* (*RSPO2*) gene that encodes the LGR5 ligand and functions as an extracellular Wnt agonist (Fig. 6B; HCCs with *RSPO2* amplification are indicated as orange and violet triangles) [53].

We used data deposited by the TCGA consortium to analyze mutations or genomic rearrangement of the *NKD1* locus in cancer tissue. Previous reports identified the *NKD1* mutations within CRCs displaying MSI [54]. However, the coding region of *NKD1* in the corresponding TCGA dataset showed that the gene was modified only marginally, with one nonsense (p.R294X), one missense (p.P230L), and one silent mutation (p.L142L) detected within CRC samples and one silent mutation (p.C248C) found in rectal cancers, respectively. In addition, TCGA CRC samples were explored using the COSMIC interface (http://cancer.sanger.ac.uk/cancergenome/projects/cosmic/). The open reading frame of *NKD1* was found to be altered by one silent (p.G312G), one missense mutation (p.A374T) and one in-frame deletion (p.K104delK). Of note, neither of the missense mutations affect the NKD1 EFX domain presumably required for the interaction with DVL proteins [27]. Moreover, unlike reported [54], the integrity of the *NKD1* exon 10 poly$(C)_7$ stretch was impaired in a single case. Moreover, the *NKD1* genomic region was never subjected to significant amplification or deletion (data not shown). In line with CRC, mutational inactivation of *NKD1* is rare in HCC, with one p.P349L substitution detected within the HCC TCGA dataset and similarly, two *NKD1* missense mutations (p.R31P and p.K116R) recorded within COSMIC data survey (827 samples).

Finally, the methylation status of the *NKD1* locus in 366 CRC samples from the TCGA dataset

was analyzed and correlated to the *NKD1* transcription level. Whereas the CpG island (and adjacent loci) proximal to the *NKD1* promoter

Fig. 2. Tracking *Nkd1* expression using Nkd1-CreERT2 BAC transgenic mice.(A) Schemes depicting the BAC clone RP23-301N2 harboring the Nkd1 locus and generation of Nkd1-CreERT2 transgenic mice. CreERT2 was inserted into the second coding exon of the *Nkd1* gene of bacteria using homologous recombination. The insertion is in frame with the translation start located in the *Nkd1* first exon. The non-coding or translated regions are indicated by empty and black boxes, respectively. a,b, *Nkd1* sequences employed for homologous recombination; RGB poly A, a poly A signal derived from the rabbit β-globulin gene; KanR, the kanamycin resistance gene; pBla, β-lactamase promoter. Prior to pronuclear injection, the bacterial resistance cassette was excised from recombinant BAC using Flp recombinase and FRT sites (violet semicircles) flanking the cassette. (B) Comparison of the whole-mount hybridization of wild-type mouse embryo at embryonic day (E) 14.5 using an antisense probe against *Nkd1* (left image) with the activity of CreERT2 recombinase produced from the Nkd1-CreERT2 BAC transgene in Nkd1-CreERT2$^+$/Rosa26R embryos obtained at the same developmental stage (right). Tamoxifen was injected intraperitoneally into pregnant females and the animals were sacrificed one day later. cb, cerebral plate; dfl, distal forelimb; dhl, distal hindlimb drg, dorsal root ganglion; ee, ear; ma, maxilla; mg, mammary gland primordium; vi, vibrissae. (C) Stereoscopic images of whole-mount staining of LacZ in different anatomical parts of the intestine of Nkd1-CreERT2$^+$/Rosa26R mice six days after tamoxifen administration. duod, duodenum; jej, jejunum; ile, ileum; col, colon. (D) Lineage tracing in the duodenum of Nkd1-CreERT2$^+$/Rosa26R mice. The LacZ activity was detected in histological specimens at indicated days after tamoxifen administration. The slides were counterstained with nuclear red. One day upon tamoxifen administration the bottom parts of the crypts were labelled (black arrowheads in the left image), whereas three weeks later cellular clones formed blue ribbons extending from the crypts to the villi (right image). In addition, the tissue contains labelled Paneth cells residing at the crypt bottom (green arrow in the left image). (E) Double labeling shows that blue cells express markers of enteroendocrine (visualized by anti-chromogranin A staining), goblet (positive for PAS), and Paneth (anti-lysozyme) cell lineages. (F) Expression of endogenous *Nkd1* in cell populations sorted from the intestinal crypts is confined to the cell types localized at the crypt bottom. Left, diagram of the sorting procedure using crypt cells isolated from the proximal half of the small intestine of three Lgr5-EGFP-IRES-CreERT2 mice. Four cell populations were obtained representing ISCs (GFP$^+$), putative precursors of Paneth and enteroendocrine cell lineages (GFP$^+$UEA$^+$), mature Paneth cells (GFP$^-$UEA$^+$), TA cells (GFP$^-$UEA$^-$). Right, qRT-PCR of sorted crypt cell populations. Cp values were normalized to *Ubb*. Means relative to values obtained in GFP$^-$UEA$^-$ cells are presented with corresponding SDs. *Crypt*, *cryptidins 1/3/6 – 12/14/15*. (G) Distribution of LacZ-positive cells in the crypts of Nkd1-CreERT2$^+$/Rosa26R mice one day after tamoxifen administration. Four hundred crypts in proximal parts of the small intestine in two mice were counted. Results are depicted as means with SDs. The cell positions are indicated in the scheme in the inset: Paneth cells ("P") are depicted in red, CBC stem cells occupy crypt positions "0" and "1", and putative Paneth cell progenitors position "2". Scale bar: 2 mm (B), 5 mm (C), 0.1 mm (D), 5 μM (E).

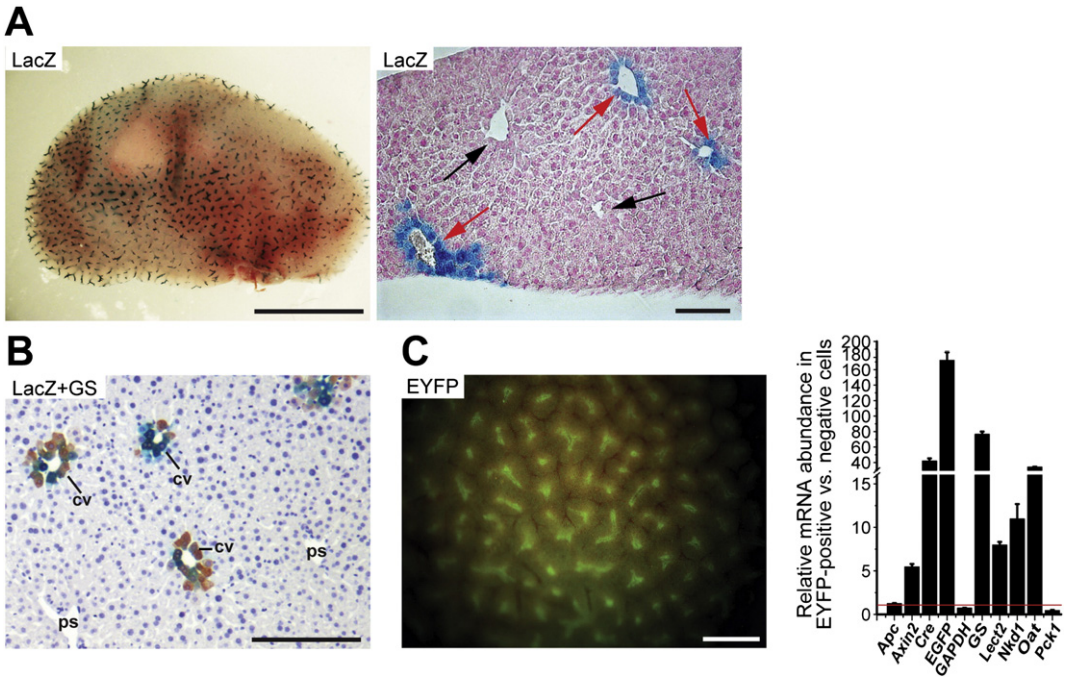

Fig. 3. *Nkd1* transcription is zonated to the perivenous hepatocytes. (A) Left, whole-mount staining of LacZ in the adult liver of Nkd1-CreERT2^{+}/Rosa26R mice one day after tamoxifen administration. Right, histochemical staining detects the LacZ activity in hepatocytes surrounding the putative centrilobular veins [(cv); red arrow]; periportal hepatocytes in close proximity to the portal space [(ps); black arrow] are LacZ negative. The specimen was counterstained with nuclear red. Scale bar: 4 mm (left image), 0.3 mm (right image). (B) Immunohistochemical co-localization of LacZ (blue color) and anti-GS (brown color) staining. The specimen was counterstained with hematoxylin. Scale bar: 0.3 mm. (C) Left, whole-mount fluorescent image of the Nkd1-CreERT2^{+}/Rosa26R-EYFP liver taken four days upon tamoxifen administration. Scale bar: 0.4 mm. Right, qRT-PCR analysis of EYFP^{+} and EYFP^{-} cells sorted from the Nkd1-CreERT2^{+}/Rosa26R-EYFP liver. The results were normalized to *Ubb* mRNA levels. The expression level of a given gene in EYFP^{-} cells was arbitrarily set to 1 (red line). Error bar: SD. Notice the enrichment of *Nkd1* mRNA along with other pericentral hepatocyte genes *Axin2*, *GS*, *Lect2*, and *Oat*. In contrast, *Apc* and *GAPDH* genes are not zonated and portal-specific *Pck1* displays a complementary expression pattern to the perivenous hepatocyte genes.

was hypomethylated in the majority of CRCs, the distal CpG island was heavily methylated. In concordance with previously published data [44] , differential methylation of the CpG island and adjacent "shores" (for terminology see Materials and Methods) situated within 2 kb of the transcription start site was strongly associated with transcription of the *NKD1* gene. Interestingly, the highest *NKD1* mRNA levels were

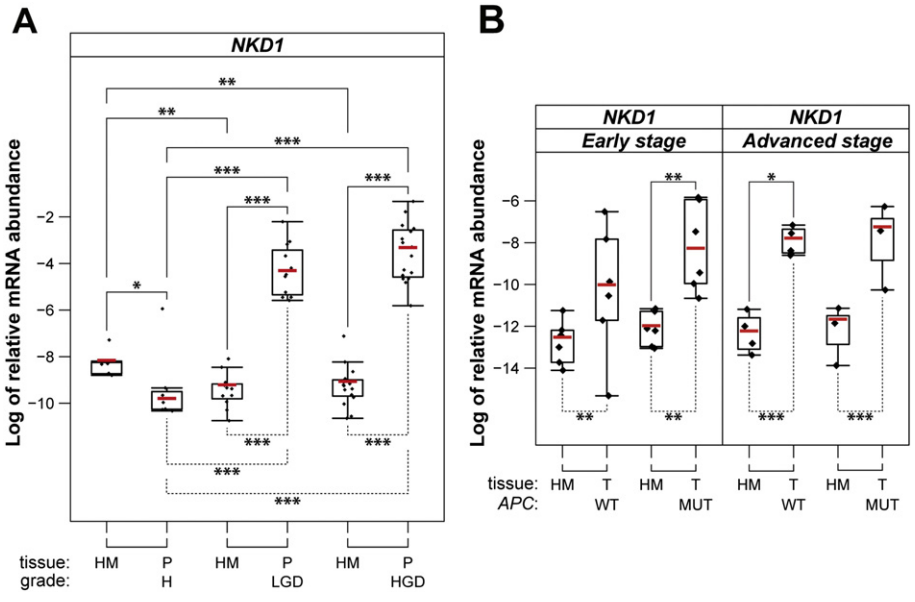

Fig. 4. NKD1 expression is increased during colorectal cancerogenesis. (A) Relative expression levels of *NKD1* in colorectal polyps. Log of relative expression levels (-ΔCp) were obtained following normalization of Cp values by geometric average of internal housekeeping genes *ACTB*, *UBB* and *AXIN1*. Predominant histological appearance stratified the lesions to hyperplasia (H), low-grade dysplasia (LGD) and high-grade dysplasia (HGD) subgroups. (B) Relative levels of *NKD1* transcript in CRCs. Cp values were normalized using *ACTB* as a reference gene to obtain ΔCp's. Malignant lesions were subdivided to distinct subgroups with respect to the *APC* mutation status (WT, wild-type *APC*; MUT, *APC* mutated) and disease progression. Statistical significance of differential expression in the given groups was examined by nonparametric Wilcoxon's rank-sum test (solid line). Moreover, the linear model (REML; dashed line), which accounted for the individual background of the patients, tissue type, histopathology, *APC* mutation status (CRC specimens only), was applied. The boxed areas correspond to the second and third quartiles; the range of the values is given by "whiskers" above and below each box. Median of ΔCp values for individual categories is depicted as the red line. Statistical data accompanying Fig. 4A and B can be found in Supplementary Table S5 and S6, respectively. *P < 0.05, **P < 0.01, and ***P < 0.001. HM, matching healthy mucosa; P, polyp; T, tumor.

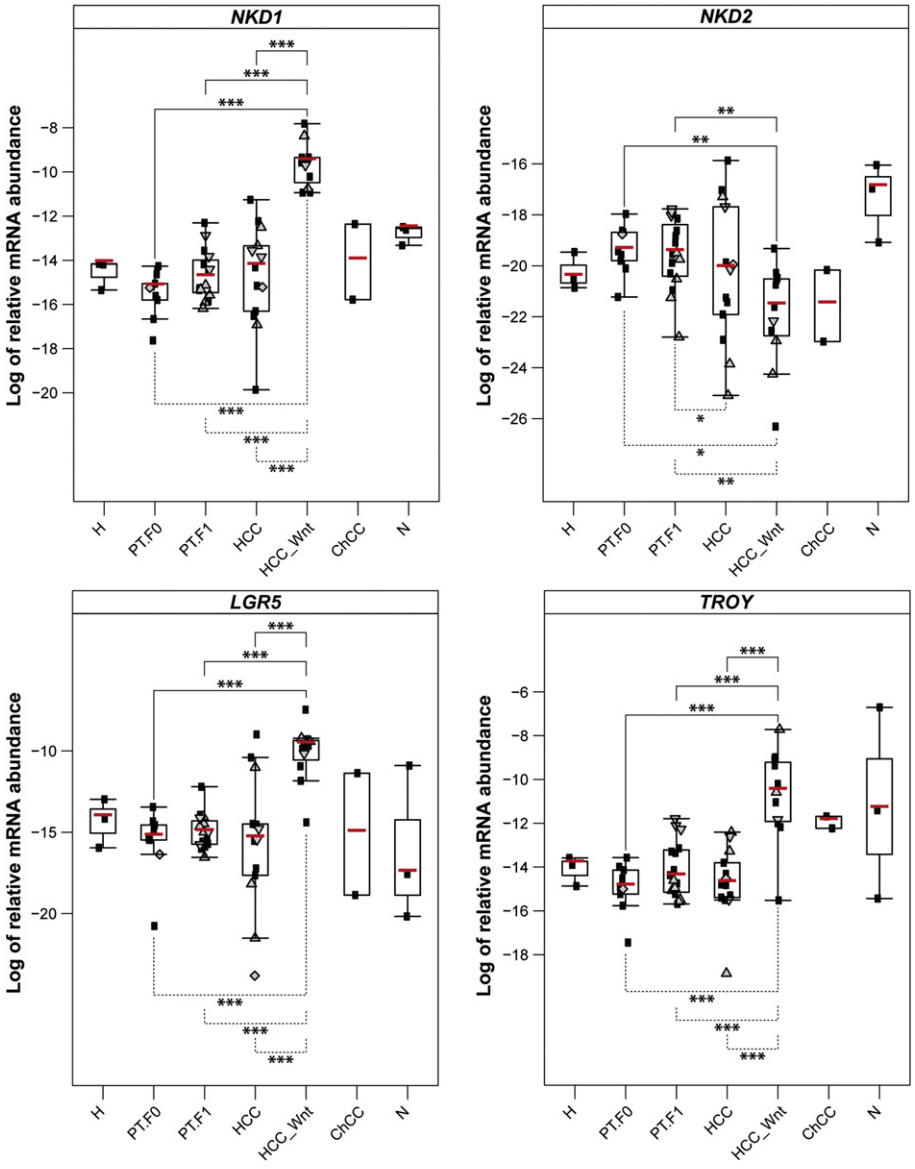

Fig. 5. NKD1 transcription is elevated in the Wnt class of HCCs. Relative mRNA abundance of the indicated genes in liver tumors and matched surrounding tissue. For each gene, Cp values were normalized by geometric average of the housekeeping genes *ACTB* and *UBB* (−ΔCp). The Wnt class (HCC_Wnt) was defined by expression levels of *AXIN2*, *EPBH2*, and *GS* genes (details are given in Supplementary Fig. S2). Two cases of cholangiocellular carcinoma constitute a separate group designated as ChCC. Additional types of liver neoplasia (adenolipoma, focal nodular hyperplasia and metastasis of colorectal carcinoma) were merged to a single group (N). Specimens of matched surrounding parenchyma were assessed according to the degree of fibrosis as healthy (H), precancerous tissue displaying mild to moderate fibrosis (PT.F0), or precancerous tissue exhibiting severe fibrosis to cirrhosis (PT.F1) [73]. Statistical significance of differential expression in the given groups was examined by nonparametric Wilcoxon's rank-sum test (solid line). Moreover, the linear model (REML; dashed line), which accounted for the individual background of the patients, tissue type and fibrosis score, was applied. The presence of viral infection is indicated by graphical symbols [circle: virus not detected; triangle: HBV positive; down-pointing triangle: HCV positive; lozenge: HBV + HCV positive]. Statistical analysis of ChCC samples was omitted from the image due to the small group size. Median of ΔCp values for individual categories is depicted as the red line. Numeric values accompanying this figure are given in Supplementary Table S7. *P < 0.05, **P < 0.01, and ***P < 0.001.

detected in CRC specimens that showed hypomethylation in the intron 3 S-shore region (Supplementary Figure S5).

4. Discussion

The activity of the Wnt pathway undergoes complex regulation to ensure proper functioning of signaling during development and in adult tissue homeostasis. The regulation may occur at several levels and includes both positive and negative feedback loops. In the intestinal crypt, a well-established cellular system depending on Wnt signaling, the pathway up-regulates Lgr5, a receptor for Rspos, and consequently, the Lgr5-Rspo interaction augments the Wnt/β-catenin signaling output [53]. In addition, Axin2 and Troy, two inhibitors of the Wnt pathway, are also induced by Wnt signaling [6,55]. Interestingly, mRNA levels encoding these genes display some variations among different cellular types located in the crypt. Troy appears to be exclusively expressed in ISCs [6,56]. However, Lgr5 – originally sought to be a unique stem cell marker – is also produced in non-dividing progenitors of the Paneth cells lineage [46]. Moreover, Axin2 expression is confined to the majority of cellular types located in the lower part of the crypts, i.e. ISCs, Paneth cells and their progenitors, and TA cells [46]. According to our lineage tracing experiments and expression analysis (Fig. 2), *Nkd1* represents another negative feedback regulator of Wnt signaling displaying relatively broad expression in the mouse crypt. Currently, it is not clear whether the observed differences in expression profiles of these Wnt pathway genes have any functional consequences. It is possible that these differences contribute to the fine-tuning of Wnt signaling. However, since targeted inactivation of any of the genes described above has no obvious phenotype, such explanation seems unlikely. More probably, random fluctuations in gene transcription might account for

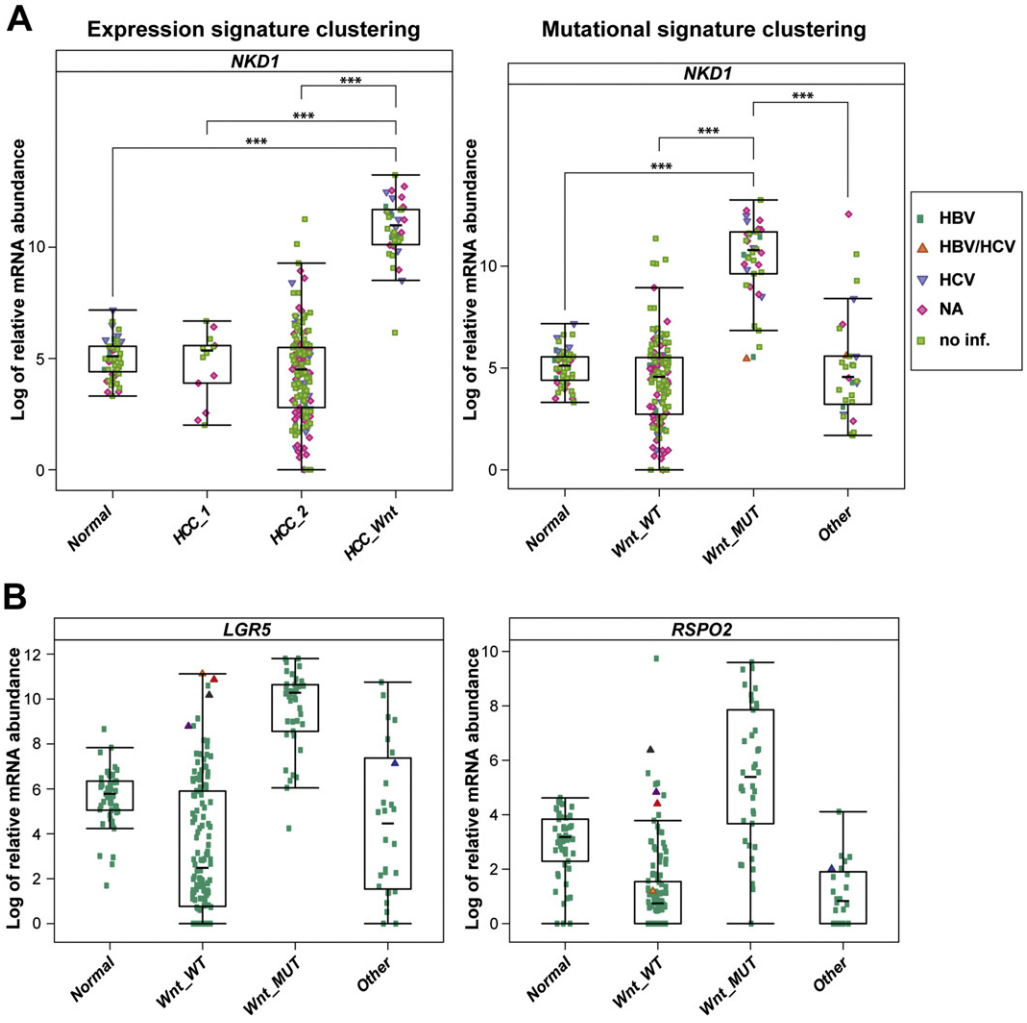

Fig. 6. NKD1 defines HCC displaying aberrant Wnt signaling. (A) Left panel, expression of *NKD1* in three gene expression classes of HCCs. The TCGA HCC specimens were stratified using transcription levels of the *AXIN2*, *EPHB2*, and *GS* (details are given in Supplementary Fig. S3). Right panel, relative expression of *NKD1* in HCC samples assigned to the individual mutation groups. Classification of the TCGA HCC specimens according to mutational changes in *APC*, *AXIN1/2*, and *CNNB1* is given in Supplementary Fig. S4. (B) Expression of *LGR5* and *RSPO2* in the HCC mutation groups. Samples assigned to the HCC_Wnt class that do not fall to the Wnt_MUT group are indicated by triangles of matched color. Black lines indicate median of expression levels for individual categories. Numerical values accompanying this figure are given in Supplementary Tables S7 and S8. *P < 0.05, **P < 0.01, and ***P < 0.001.

the observed variations in mRNA levels of a given gene in crypt cells [57] . In the mouse liver, *Nkd1* represents, together with *Axin2* and *Troy* (BF and VK, unpublished data), a robust marker of perivenous hepatocytes. Although the involvement of Wnt signaling in liver zonation is well established, the liver-specific *Nkd1* function has not been – similarly as in gut tissue – documented.

In a collection of human intestinal neoplasia the *NKD* mRNA levels were upregulated in nearly all of the tumors irrespective of the *APC* status (Fig. 4). This was seemingly surprising, since in mouse hyperplastic crypts *Nkd1* overexpression was directly linked to *Apc* loss. Nevertheless, the mutational status of *APC* in the panel of CRCs was based on sequencing of the exon 19 (NCBI nomenclature) that contains the mutational "hot spot", but it likely does not cover all *APC* mutations [6]. Moreover, recent studies employing massive parallel sequencing of tumor DNA indicated that gene alterations resulting in hyperactive Wnt signaling can be found in more than 90% of CRCs [18]. Therefore, limited knowledge of the status of the Wnt pathway in (our) CRC collection can be attributed to the discrepancy between *Nkd1* expression data obtained in the mouse and in clinical samples. This explanation may interpret the observed decrease in the *NKD1* mRNA levels in hyperplastic polyps (Fig. 4A). According to the recent concept of the "serrated neoplasia pathway", precancerous hyperplasia is linked to the development of a separate subclass of gut tumors [58]. Serrated CRC lesions are predominantly initiated by oncogenic *BRAF* mutations and do not harbor genetic changes that would compromise control over Wnt signaling [59].

Relevant CRC datasets obtained from TCGA did not include paired samples of the healthy mucosa, and thus we could not directly compare the *NKD1* mRNA levels in tumors and normal (matched) tissue. Nevertheless, in APC-deficient CRCs at early stage of progression, *NKD1* transcription was higher in MSS lesions than in tumors displaying increased levels of microsatellite instability. Furthermore, upon subdivision of CRCs according to their expression signature, *NKD1* mRNA was significantly increased in the TA (progenitor) type of the tumors (Supplementary Fig. S1). Whether the extent of *NKD1* upregulation reflects a particular mechanism of tumor initiation or mirrors the variability of *NKD1* expression in the cellular types present in the healthy colon remains to be determined.

Although in the majority of CRCs the aberrant Wnt activity is attributable to mutations affecting intracellular components of the Wnt pathway [18], the signaling output can be augmented by epigenetic silencing of genes encoding secreted Wnt antagonists, such as secreted frizzled-related proteins (SFRPs) and dickkopf WNT signaling pathway inhibitors (DKKs) [60–63]. Thus, integration of genetic and epigenetic changes that affect multiple steps of the Wnt signal transduction likely confers a selective advantage to tumor cells. In line with these "multiple-hit"

concepts and given that methylation of *NKD1* regulatory elements was observed in ovarian and gastric cancer [64,65], we investigated the methylation status in 366 CRC samples of the TCGA dataset and examined its relation to *NKD1* transcription. In contrast to other neoplasia, loci proximal to the *NKD1* promoter were unmethylated. Moreover, *NKD1* mRNA was more abundant in colorectal tumors displaying hypomethylation in the S-shore region located in the third intron of the *NKD1* gene (Supplementary Figure S5). Strikingly, the CRC "methylome" analysis by Irizarry and colleagues identified an identical inverse relationship between intron 3 S-shore methylation and *NKD1* expression [44]. In summary, dysregulation of *NKD1* in tumors is possibly driven by as yet undescribed epigenetic mechanisms.

The etiology of HCC is mainly associated with alcohol abuse and HBV and HCV infection. Consequently, HCC is rather a heterogeneous disease and the link between aberrant Wnt signaling and HCC is less obvious than in the cancer of the colon and rectum. Although there is no generally accepted molecular classification of the disease, several recent studies identified (sub)classes of HCC. Importantly, the Wnt-associated class of HCC (approximately 20–40% of all cases) is predominantly defined by the presence of activating mutations in the *CTNNB1* gene. In contrast, alterations in *APC*, so dominant in CRC, are less frequent in HCC (2–3%) [66]. This is rather peculiar since the *APC* gene represents a substantially larger "target" than the exon 3 in the *CTNNB1* gene. Of note, in hepatoblastoma, the most frequent malignant pediatric tumor of the liver, approximately 50% of neoplastic lesions harbor activating mutation in *CTNNB1* [67] and display elevated expression of *NKD1* [68]. Nevertheless, since *APC* and *CTNNB1* mutations are mutually exclusive, the high frequency of the changes in the latter gene possibly reflects a combination of the locus accessibility and/or presence of liver-specific mutagens rather than any unique β-catenin-dependent role in HCC initiation or progression.

The gene expression signature of three Wnt signaling target genes, *AXIN2*, *EPHB2*, and *GS*, was used to stratify HCCs to the β-catenin-dependent "HCC_Wnt" class. Although we were unable (probably due to the limited number of specimens in our experimental collection) to separate the rest of the samples to other classes as described previously [25], the *NKD1* expression profile fitted well to the "HCC_Wnt" class. In agreement with these results, bioinformatic analysis of the HCC datasets obtained from TCGA confirmed that *AXIN2*, *EPHB2*, *GS*, and *NKD1* represent robust markers of the HCC_Wnt class. Interestingly, not all specimens from this class harbored mutations in the *APC*, *AXIN1/2*, and *CTNNB1* genes. Interestingly, we observed amplification of the *RSPO2* locus in two of the samples (out of four in total). This is in accordance with recent data indicating that the amplification of the *RSPO* genes represents a frequent event in HCC (up to 25%) [51–66]. Increased production of *RSPO* ligands has been observed in CRC as an oncogenic "by-pass" mechanism that circumvents intact *APC* [69]. Collectively, the membranous inputs may contribute to liver tumorigenesis in a manner analogous to signaling circuits described in CRC. Finally, seven samples assigned to the Wnt_MUT group did not display the Wnt-dependent expression signature. Since all these samples carried "likely oncogenic mutations" (LOMs) in exon 3 of the *CTNNB1* (Supplementary Table S4) that do not change the regulatory serine/threonine residue, we presume that these mutations are "passenger" without any effect on the β-catenin stability.

Simultaneous inactivation of *APC* and *AXIN2* or *APC* and *NKD1* occurs in exceptional cases only. Since sustained expression of *AXIN2* and *NKD1* is typical of APC-deficient tumors, we speculate that the function of these Wnt pathway inhibitors might be strongly favored to keep the Wnt pathway activity "optimal" for tumor growth [70,71]. This conclusion is in accordance with recent results of Barrry and colleagues demonstrating that another DVL interacting partner, yes-associated protein 1 (YAP1), limits aberrant Wnt signaling and that YAP1-deficiency leads to highly aggressive undifferentiated CRCs or results in Wnt hypersensitivity during intestinal regeneration [72]. Interestingly, YAP1 restricts Wnt signaling independently of the β-catenin destruction complex by suppressing nuclear translocation of Dvl. Thus, we propose that in concordance with the "passive antagonist" model [32], Nkd1 might directly influence the nuclear Dvl function in cells displaying hyperactive Wnt signaling.

In summary, despite its unclear molecular function, *NKD1* can serve as a reliable marker of intestinal and liver tumors that display aberrant Wnt/β-catenin signaling.

5. Conclusion

Mutations in genes encoding components of the Wnt/β-catenin pathway that result in aberrant activation of the signaling are undoubtedly linked to the onset of intestinal cancer. In contrast, the etiology of liver cancer is heterogeneous and frequently linked to viral infection. Although several recent studies aimed to identify subclasses of HCC, there is no generally accepted molecular classification of the disease. In the present study we employed a negative feedback regulator of Wnt signaling, Nkd1, as a marker of active Wnt signaling in the intestine and liver and in tumors originating from these organs. Our results provide evidence that *NKD1* can be utilized to distinguish a class of HCC linked to aberrant Wnt signaling.

Conflicts of interest

There are no conflicts of interest to disclose.

Acknowledgements

We thank S. Takacova for critically reading the manuscript. We also thank M. Cepko and S. Robine for reagents and Villin-CreERT2 mice. This work was supported by the Grant Agency of the Czech Republic (Grant No. P305/11/1780), institutional grant from the Academy of Sciences of the Czech Republic (RVO 68378050), project BIOCEV – Biotechnology and Biomedicine Centre of the Academy of Sciences and Charles University (CZ.1.05/1.1.00/02.0109) from the European Regional Development Fund to V.K. and R.S., Ministry of Education, Youth and Sports of the Czech Republic (LM2011032) to R.S., Institutional support from the Ministry of Health of the Czech Republic for development of research organization (00023001) to M.O., M.N., and M.J., Grant Agency of Charles University in Prague (1400-243-253470) to J.St., Charles University in Prague Research Project PRVOUK - Oncology P27 to J.Sv.

The results shown here are in part based upon data generated by the TCGA Research (http://cancergenome.nih.gov/). We are deeply grateful to all specimen donors and research groups that have made the data publicly available. We also express our special thanks to the employees of the Transgenic and Archiving Module, the Czech Centre for Phenogenomics, IMG, Prague for their excellent effort in generation of transgenic mice.

Appendix A. Supplementary data

Supplementary data to this article can be found online at http://dx.doi.org/10.1016/j.cellsig.2014.11.008.

References

[1] K.M. Cadigan, Cold Spring Harb. Perspect. Biol. 1 (2009) a002881.
[2] T. Valenta, G. Hausmann, K. Basler, EMBO J. 31 (2012) 2714–2736.
[3] A. Schepers, H. Clevers, Cold Spring Harb. Perspect. Biol. 4 (2012) a007989.
[4] H.C. Clevers, C.L. Bevins, Annu. Rev. Physiol. 75 (2013) 289–311.
[5] N. Barker, J.H. van Es, J. Kuipers, P. Kujala, M. van den Born, M. Cozijnsen, A. Haegebarth, J. Korving, H. Begthel, P.J. Peters, H. Clevers, Nature 449 (2007) 1003–1007.
[6] B. Fafilek, M. Krausova, M. Vojtechova, V. Pospichalova, L. Tumova, E. Sloncova, M. Huranova, J. Stancikova, A. Hlavata, J. Svec, R. Sedlacek, O. Luksan, M. Oliverius, L. Voska, M. Jirsa, J. Paces, M. Kolar, M. Krivjanska, K. Klimesova, H. Tlaskalova-Hogenova, V. Korinek, Gastroenterology 144 (2013) 381–391.

[7] L.G. van der Flier, M.E. van Gijn, P. Hatzis, P. Kujala, A. Haegebarth, D.E. Stange, H. Begthel, M. van den Born, V. Guryev, I. Oving, J.H. van Es, N. Barker, P.J. Peters, M. van de Wetering, H. Clevers, Cell 136 (2009) 903–912.
[8] E. Batlle, J.T. Henderson, H. Beghtel, M.M. van den Born, E. Sancho, G. Huls, J. Meeldijk, J. Robertson, M. van de Wetering, T. Pawson, H. Clevers, Cell 111 (2002) 251–263.
[9] M. Krausova, V. Korinek, Cell. Signal. 26 (2014) 570–579.
[10] V. Korinek, N. Barker, P. Moerer, E. van Donselaar, G. Huls, P.J. Peters, H. Clevers, Nat. Genet. 19 (1998) 379–383.
[11] J.H. van Es, A. Haegebarth, P. Kujala, S. Itzkovitz, B.K. Koo, S.F. Boj, J. Korving, M. van den Born, A. van Oudenaarden, S. Robine, H. Clevers, Mol. Cell. Biol. 32 (2012) 1918–1927.
[12] T. Fevr, S. Robine, D. Louvard, J. Huelsken, Mol. Cell. Biol. 27 (2007) 7551–7559.
[13] H. Ireland, R. Kemp, C. Houghton, L. Howard, A.R. Clarke, O.J. Sansom, D.J. Winton, Gastroenterology 126 (2004) 1236–1246.
[14] S.P. Monga, Gene Expr. 16 (2014) 51–62.
[15] S. Benhamouche, T. Decaens, C. Godard, R. Chambrey, D.S. Rickman, C. Moinard, M. Vasseur-Cognet, C.J. Kuo, A. Kahn, C. Perret, S. Colnot, Dev. Cell 10 (2006) 759–770.
[16] P. Polakis, Cold Spring Harb. Perspect. Biol. 4 (2012).
[17] K.W. Kinzler, B. Vogelstein, Cell 87 (1996) 159–170.
[18] Nature 487 (2012) 330–337.
[19] D.P. Minde, Z. Anvarian, S.G. Rudiger, M.M. Maurice, Mol. Cancer 10 (2011) 101.
[20] Y. Shimizu, S. Ikeda, M. Fujimori, S. Kodama, M. Nakahara, M. Okajima, T. Asahara, Genes Chromosom. Cancer 33 (2002) 73–81.
[21] W. Liu, X. Dong, M. Mai, R.S. Seelan, K. Taniguchi, K.K. Krishnadath, K.C. Halling, J.M. Cunningham, L.A. Boardman, C. Qian, E. Christensen, S.S. Schmidt, P.C. Roche, D.I. Smith, S.N. Thibodeau, Nat. Genet. 26 (2000) 146–147.
[22] P.J. Morin, A.B. Sparks, V. Korinek, N. Barker, H. Clevers, B. Vogelstein, K.W. Kinzler, Science 275 (1997) 1787–1790.
[23] H.B. El-Serag, K.L. Rudolph, Gastroenterology 132 (2007) 2557–2576.
[24] Y. Hoshida, S.M. Nijman, M. Kobayashi, J.A. Chan, J.P. Brunet, D.Y. Chiang, A. Villanueva, P. Newell, K. Ikeda, M. Hashimoto, G. Watanabe, S. Gabriel, S.L. Friedman, H. Kumada, J.M. Llovet, T.R. Golub, Cancer Res. 69 (2009) 7385–7392.
[25] A. Lachenmayer, C. Alsinet, R. Savic, L. Cabellos, S. Toffanin, Y. Hoshida, A. Villanueva, B. Minguez, P. Newell, H.W. Tsai, J. Barretina, S. Thung, S.C. Ward, J. Bruix, V. Mazzaferro, M. Schwartz, S.L. Friedman, J.M. Llovet, Clin. Cancer Res. 18 (2012) 4997–5007.
[26] S. Li, M. Mao, Cancer Lett. 340 (2013) 247–253.
[27] R. Rousset, J.A. Mack, K.A. Wharton Jr., J.D. Axelrod, K.M. Cadigan, M.P. Fish, R. Nusse, M.P. Scott, Genes Dev. 15 (2001) 658–671.
[28] I. Schneider, P.N. Schneider, S.W. Derry, S. Lin, L.J. Barton, T. Westfall, D.C. Slusarski, Dev. Biol. 348 (2010) 22–33.
[29] T.J. Van Raay, R.J. Coffey, L. Solnica-Krezel, Dev. Biol. 309 (2007) 151–168.
[30] T.J. Van Raay, N.J. Fortino, B.W. Miller, H. Ma, G. Lau, C. Li, J.L. Franklin, L. Attisano, L. Solnica-Krezel, R.J. Coffey, PLoS One 6 (2011) e18650.
[31] S. Zhang, T. Cagatay, M. Amanai, M. Zhang, J. Kline, D.H. Castrillon, R. Ashfaq, O.K. Oz, K.A. Wharton Jr., Mol. Cell. Biol. 27 (2007) 4454–4464.
[32] D. Angonin, T.J. Van Raay, PLoS One 8 (2013) e74666.
[33] A.R. Moser, H.C. Pitot, W.F. Dove, Science 247 (1990) 322–324.
[34] L.K. Su, K.W. Kinzler, B. Vogelstein, A.C. Preisinger, A.R. Moser, C. Luongo, K.A. Gould, W.F. Dove, Science 256 (1992) 668–670.
[35] P. Soriano, Nat. Genet. 21 (1999) 70–71.
[36] S. Srinivas, T. Watanabe, C.S. Lin, C.M. William, Y. Tanabe, T.M. Jessell, F. Costantini, BMC Dev. Biol. 1 (4) (2001).
[37] M. Kuraguchi, X.P. Wang, R.T. Bronson, R. Rothenberg, N.Y. Ohene-Baah, J.J. Lund, M. Kucherlapati, R.L. Maas, R. Kucherlapati, PLoS Genet. 2 (2006) e146.
[38] F. el Marjou, K.P. Janssen, B.H. Chang, M. Li, V. Hindie, L. Chan, D. Louvard, P. Chambon, D. Metzger, S. Robine, Genesis 39 (2004) 186–193.
[39] T. Shimosato, M. Tohno, T. Sato, J. Nishimura, Y. Kawai, T. Saito, H. Kitazawa, Anim. Sci. J. 80 (2009) 597–604.
[40] O. Machon, C.J. van den Bout, M. Backman, O. Rosok, X. Caubit, S.H. Fromm, B. Geronimo, S. Krauss, Neuroscience 112 (2002) 951–966.
[41] T. Sato, J.H. van Es, H.J. Snippert, D.E. Stange, R.G. Vries, M. van den Born, N. Barker, N.F. Shroyer, M. van de Wetering, H. Clevers, Nature 469 (2011) 415–418.
[42] Y. Ohashi, S. Kansal, M. Schreiber Jr., Advances in peritoneal dialysis, Conference on peritoneal dialysis282012. 131–133.
[43] H. Wu, B. Caffo, H.A. Jaffee, R.A. Irizarry, A.P. Feinberg, Biostatistics 11 (2010) 499–514.
[44] R.A. Irizarry, C. Ladd-Acosta, B. Wen, Z. Wu, C. Montano, P. Onyango, H. Cui, K. Gabo, M. Rongione, M. Webster, H. Ji, J.B. Potash, S. Sabunciyan, A.P. Feinberg, Nat. Genet. 41 (2009) 178–186.
[45] A.E. Powell, Y. Wang, Y. Li, E.J. Poulin, A.L. Means, M.K. Washington, J.N. Higginbotham, A. Juchheim, N. Prasad, S.E. Levy, Y. Guo, Y. Shyr, B.J. Aronow, K.M. Haigis, J.L. Franklin, R.J. Coffey, Cell 149 (2012) 146–158.
[46] S.J. Buczacki, H.I. Zecchini, A.M. Nicholson, R. Russell, L. Vermeulen, R. Kemp, D.J. Winton, Nature 495 (2013) 65–69.
[47] A. Sadanandam, C.A. Lyssiotis, K. Homicsko, E.A. Collisson, W.J. Gibb, S. Wullschleger, L.C. Ostos, W.A. Lannon, C. Grotzinger, M. Del Rio, B. Lhermitte, A.B. Olshen, B. Wiedenmann, L.C. Cantley, J.W. Gray, D. Hanahan, Nat. Med. 19 (2013) 619–625.
[48] C. Fraley, A.E. Raftery, J. Classif. 20 (2003) 263–286.
[49] O.N. Ikediobi, H. Davies, G. Bignell, S. Edkins, C. Stevens, S. O'Meara, T. Santarius, T. Avis, S. Barthorpe, L. Brackenbury, G. Buck, A. Butler, J. Clements, J. Cole, E. Dicks, S. Forbes, K. Gray, K. Halliday, R. Harrison, K. Hills, J. Hinton, C. Hunter, A. Jenkinson, D. Jones, V. Kosmidou, R. Lugg, A. Menzies, T. Mironenko, A. Parker, J. Perry, K. Raine, D. Richardson, R. Shepherd, A. Small, R. Smith, H. Solomon, P. Stephens, J. Teague, C. Tofts, J. Varian, T. Webb, S. West, S. Widaa, A. Yates, W. Reinhold, J.N. Weinstein, M.R. Stratton, P.A. Futreal, R. Wooster, Mol. Cancer Ther. 5 (2006) 2606–2612.
[50] G.R. Bignell, C.D. Greenman, H. Davies, A.P. Butler, S. Edkins, J.M. Andrews, G. Buck, L. Chen, D. Beare, C. Latimer, S. Widaa, J. Hinton, C. Fahey, B. Fu, S. Swamy, G.L. Dalgliesh, B.T. Teh, P. Deloukas, F. Yang, P.J. Campbell, P.A. Futreal, M.R. Stratton, Nature 463 (2010) 893–898.
[51] C. Guichard, G. Amaddeo, S. Imbeaud, Y. Ladeiro, L. Pelletier, I.B. Maad, J. Calderaro, P. Bioulac-Sage, M. Letexier, F. Degos, B. Clement, C. Balabaud, E. Chevet, A. Laurent, G. Couchy, E. Letouze, F. Calvo, J. Zucman-Rossi, Nat. Genet. 44 (2012) 694–698.
[52] V.H. Bustos, A. Ferrarese, A. Venerando, O. Marin, J.E. Allende, L.A. Pinna, Proc. Natl. Acad. Sci. U. S. A. 103 (2006) 19725–19730.
[53] W. de Lau, N. Barker, T.Y. Low, B.K. Koo, V.S. Li, H. Teunissen, P. Kujala, A. Haegebarth, P.J. Peters, M. van de Wetering, D.E. Stange, J.E. van Es, D. Guardavaccaro, R.B. Schasfoort, Y. Mohri, K. Nishimori, S. Mohammed, A.J. Heck, H. Clevers, Nature 476 (2011) 293–297.
[54] J. Guo, T. Cagatay, G. Zhou, C.C. Chan, S. Blythe, K. Suyama, L. Zheng, K. Pan, C. Qian, R. Hamelin, S.N. Thibodeau, P.S. Klein, K.A. Wharton, W. Liu, PLoS One 4 (2009) e7982.
[55] B. Lustig, B. Jerchow, M. Sachs, S. Weiler, T. Pietsch, U. Karsten, M. van de Wetering, H. Clevers, P.M. Schlag, W. Birchmeier, J. Behrens, Mol. Cell. Biol. 22 (2002) 1184–1193.
[56] D.E. Stange, B.K. Koo, M. Huch, G. Sibbel, O. Basak, A. Lyubimova, P. Kujala, S. Bartfeld, J. Koster, J.H. Geahlen, P.J. Peters, J.H. van Es, M. van de Wetering, J.C. Mills, H. Clevers, Cell 155 (2013) 357–368.
[57] S. Itzkovitz, A. Lyubimova, I.C. Blat, M. Maynard, J. van Es, J. Lees, T. Jacks, H. Clevers, A. van Oudenaarden, Nat. Cell Biol. 14 (2012) 106–114.
[58] E.M.F. De Sousa, X. Wang, M. Jansen, E. Fessler, A. Trinh, L.P. de Rooij, J.H. de Jong, O.J. de Boer, R. van Leersum, M.F. Bijlsma, H. Rodermond, M. van der Heijden, C.J. van Noesel, J.B. Tuynman, E. Dekker, F. Markowetz, J.P. Medema, L. Vermeulen, Nat. Med. 19 (2013) 614–618.
[59] K.S. Boparai, E. Dekker, M.M. Polak, A.R. Musler, S. van Eeden, C.J. van Noesel, Am. J. Pathol. 178 (2011) 2700–2707.
[60] H. Suzuki, E. Gabrielson, W. Chen, R. Anbazhagan, M. van Engeland, M.P. Weijenberg, J.G. Herman, S.B. Baylin, Nat. Genet. 31 (2002) 141–149.
[61] A. Bafico, G. Liu, L. Goldin, V. Harris, S.A. Aaronson, Cancer Cell 6 (2004) 497–506.
[62] H. Suzuki, D.N. Watkins, K.W. Jair, K.E. Schuebel, S.D. Markowitz, W.D. Chen, T.P. Pretlow, B. Yang, Y. Akiyama, M. Van Engeland, M. Toyota, T. Tokino, Y. Hinoda, K. Imai, J.G. Herman, S.B. Baylin, Nat. Genet. 36 (2004) 417–422.
[63] Q.J. Voorham, J. Janssen, M. Tijssen, S. Snellenberg, S. Mongera, N.C. van Grieken, H. Grabsch, M. Kliment, B.J. Rembacken, C.J. Mulder, M. van Engeland, G.A. Meijer, R.D. Steenbergen, B. Carvalho, BMC Cancer 13 (2013) 603.
[64] W. Dai, J.M. Teodoridis, C. Zeller, J. Graham, J. Hersey, J.M. Flanagan, E. Stronach, D.W. Millan, N. Siddiqui, J. Paul, R. Brown, Clin. Cancer Res. 17 (2011) 4052–4062.
[65] Y. Yoda, H. Takeshima, T. Niwa, J.G. Kim, T. Ando, R. Kushima, T. Sugiyama, H. Katai, H. Noshiro, T. Ushijima, Gastric Cancer (2014), http://dx.doi.org/10.1007/s10120-014-0348-0.
[66] Z. Kan, H. Zheng, X. Liu, S. Li, T.D. Barber, Z. Gong, H. Gao, K. Hao, M.D. Willard, J. Xu, R. Hauptschein, P.A. Rejto, J. Fernandez, G. Wang, Q. Zhang, B. Wang, R. Chen, J. Wang, N.P. Lee, W. Zhou, Z. Lin, Z. Peng, K. Yi, S. Chen, L. Li, X. Fan, J. Yang, R. Ye, J. Ju, K. Wang, H. Estrella, S. Deng, P. Wei, M. Qiu, I.H. Wulur, J. Liu, M.E. Ehsani, C. Zhang, A. Loboda, W.K. Sung, A. Aggarwal, R.T. Poon, S.T. Fan, J. Wang, J. Hardwick, C. Reinhard, H. Dai, Y. Li, J.M. Luk, M. Mao, Genome Res. 23 (2013) 1422–1433.
[67] A. Koch, D. Denkhaus, S. Albrecht, I. Leuschner, D. von Schweinitz, T. Pietsch, Cancer Res. 59 (1999) 269–273.
[68] A. Koch, A. Waha, W. Hartmann, A. Hrychyk, U. Schuller, K.A. Wharton Jr., S.Y. Fuchs, D. von Schweinitz, T. Pietsch, Clin. Cancer Res. 11 (2005) 4295–4304.
[69] S. Seshagiri, E.W. Stawiski, S. Durinck, Z. Modrusan, E.E. Storm, C.B. Conboy, S. Chaudhuri, Y. Guan, V. Janakiraman, B.S. Jaiswal, J. Guillory, C. Ha, G.J. Dijkgraaf, J. Stinson, F. Gnad, M.A. Huntley, J.D. Degenhardt, P.M. Haverty, R. Bourgon, W. Wang, H. Koeppen, R. Gentleman, T.K. Starr, Z. Zhang, D.A. Largaespada, T.D. Wu, F.J. de Sauvage, Nature 488 (2012) 660–664.
[70] A. Lewis, S. Segditsas, M. Deheragoda, P. Pollard, R. Jeffery, E. Nye, H. Lockstone, H. Davis, S. Clark, G. Stamp, R. Poulsom, N. Wright, I. Tomlinson, Gut 59 (2010) 1680–1686.
[71] S.H. Chandra, I. Wacker, U.K. Appelt, J. Behrens, J. Schneikert, PLoS One 7 (2012) e34479.
[72] E.R. Barry, T. Morikawa, B.L. Butler, K. Shrestha, R. de la Rosa, K.S. Yan, C.S. Fuchs, S.T. Magness, R. Smits, S. Ogino, C.J. Kuo, F.D. Camargo, Nature 493 (2013) 106–110.
[73] K. Ishak, A. Baptista, L. Bianchi, F. Callea, J. De Groote, F. Gudat, H. Denk, V. Desmet, G. Korb, R.N. MacSween, et al., J. Hepatol. 22 (1995) 696–699.